10.051103/IJSET.251220207
Vol.21 Iss.2 pp.70-87 **International Journal of Scientific Research & Engineering Technology (IJSET)**

Optimization of active layer thicknesses for the enhancement of conversion efficiency in resonant photovoltaic cells under multi-spectral illumination

Césaire Ngor Ndiaye, Abdoulaye Sène, Fatou Kiné Mbaye, Ousmane Ndiaye, Ababacar Ndiaye et Lamine Thiaw
Ecole Supérieure Polytechnique de Dakar, Université Cheikh Anta Diop de Dakar, SENEGAL
cesairengor.ndiaye@esp.sn
abdoulaye37.sene@ucad.edu.sn
mbfatoukine@ept.sn
ousmanendiaye704@gmail.com
ababacar.ndiaye@esp.sn
lamine.thiaw@ucad.edu.sn

***Abstract*— To overcome the efficiency limitations of conventional photovoltaic cells, research has shifted toward novel materials, specifically III-V nitrides. Among these, Indium Gallium Nitride (InGaN) is particularly promising due to its tunable energy bandgap covering the entire visible spectrum, its high absorption coefficient, and its resilience to high power densities. These properties make it an outstanding candidate for high-efficiency photovoltaic solar cells. Within this framework, a resonant multi-dielectric multilayer structure has been proposed to amplify the optical field prior to its interaction with the cell's active layer, thereby enhancing absorption. This resonant structure was subsequently coupled to a single-junction InGaN cell and simulated under $AM_{1.5G}$ illumination in a steady-state regime using Matlab/Simulink. The study then proceeded to optimize the performance of the coupled cell by analyzing the influence of emitter and base thicknesses on the device's electrical parameters. The results demonstrate a significant performance enhancement: the proposed cell exhibits a higher current density (rising from 32.68 mA/cm² to 41.2 mA/cm²), a slightly improved open-circuit voltage (from 0.94 V to 0.962 V), and a substantially higher conversion efficiency, increasing from 26.5% to 34.54%. These findings suggest that this approach could pave the way for the development of significantly more efficient solar panels in the future.**

***Keywords*— In.Ga.N, Solar cells, single-junction, resonant structure, coupling, optimization, thicknesses, steady-state regime**

I. INTRODUCTION

Energy lies at the heart of the economic and technological development of modern societies. Since the Industrial Revolution, global energy demand has grown steadily, largely met by fossil fuels such as oil, coal, and natural gas [1]. While these sources have long accounted for nearly all energy production, their environmental impact—particularly regarding greenhouse gas emissions coupled with their finite and non-renewable nature, has led to a global awareness of the urgent need to diversify energy sources [2].

In this context, renewable energies are playing an increasingly central role in energy strategies. Among them, solar photovoltaic (PV) energy stands out due to its abundance, cleanliness, and virtually unlimited potential [3]. However, despite its numerous advantages, the conversion efficiency of photovoltaic cells which measures their ability to transform solar energy into electricity remains a major challenge. Conventional solar cells, primarily silicon-based, achieve efficiencies that are limited by intrinsic constraints such as spectral absorption mismatch and recombination losses [4], [5].

To overcome these limitations, extensive research is underway to enhance the performance of photovoltaic devices. One of the most promising avenues involves the use of novel materials with wide bandgaps and high absorption potential, such as III-V nitrides, specifically Indium Gallium Nitride (InGaN). This material exhibits compelling optoelectronic properties, including a tunable bandgap and excellent thermal stability, making it an ideal candidate for next-generation photovoltaic cells [6], [7].

In parallel, the optical engineering of these devices, specifically light-trapping techniques, aims to maximize photonic absorption without compromising the electrical properties of the cell [8].

ISSN: 2356-5608

10.051103/IJSET.251220207
Vol.21 Iss.2 pp.70-87 **International Journal of Scientific Research & Engineering Technology (IJSET)**

This study falls within this dual framework of enhancing photovoltaic efficiency through the integration of innovative materials, such as InGaN, and the optimization of light-trapping mechanisms.

This paper aims to model and simulate a single-junction solar cell based on Indium Gallium Nitride (InGaN), coupled with dielectric nanostructures to enhance the optical field under multi-spectral illumination in a steady-state regime. The study also focuses on optimizing the cell's electrical performance by adjusting the thickness of its various layers, using Matlab/Simulink software.

II. DESCRIPTION OF THE STUDIED MODEL

In this analysis, we investigate the optoelectronic behavior of a single-junction photovoltaic cell, composed of an $In_xGa_{1-x}N$ alloy and integrated into a multilayer dielectric resonant structure. As illustrated in Figure 1, the structure is stacked along the z-axis, which defines the depth. Since the dimensions in the x and y planes are significantly larger than the cell thickness, the lateral current components can be neglected within the scope of this one-dimensional modeling.

The optical device consists of a glass superstrate (n_0 = 1.52), a periodic stack of alternating dielectric thin films with high refractive index (n_H = 2.141, Ta_2O_5) and low refractive index (n_B = 1.4570, SiO_2), and an air substrate (n_s = 1). This architecture forms a resonant cavity designed to enhance spectral absorption within the active region of the cell.

The $In_xGa_{1-x}N$-based cell consists of three functional layers: a surface anti-reflective coating, a p-doped emitter, and an n-doped base, consistent with the conventional configuration of thin-film solar cells.

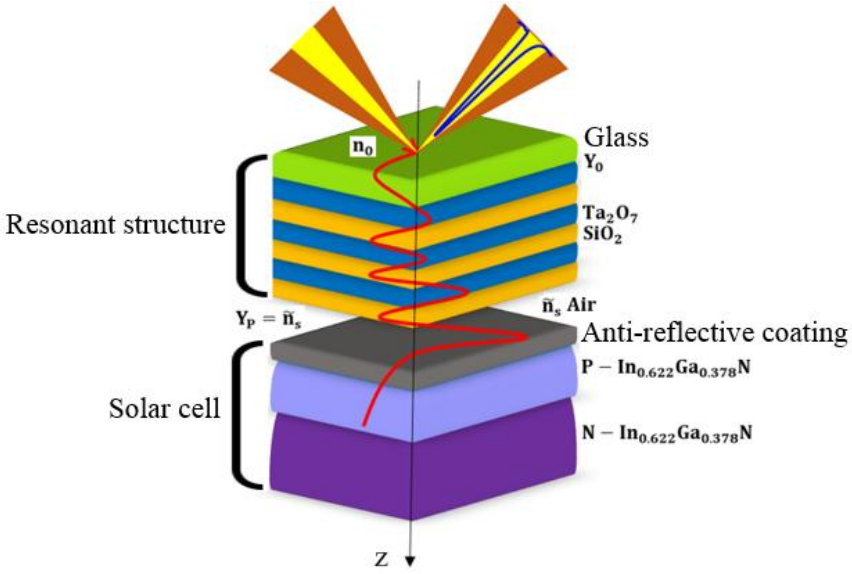

Fig. 1 Single-junction solar cell based on InGaN coupled with a resonant structure

III. SOLAR CELL MODELING

With the aim of improving solar cell efficiency, particular attention can be paid to their configuration, which plays a pivotal role in their overall performance.

A. Irradiance, incident power, and ground-level solar flux

For analytical calculation purposes, the ground-level solar irradiance is approximated by a non-linear function of the form [9] :

$$ECL(\lambda) = y_0 + A\left[1 - e^{\frac{-(\lambda-\lambda_0)}{t_1}}\right]^p e^{\frac{-(\lambda-\lambda_0)}{t_2}} \quad (1)$$

Where : λ ranges from 0.3 µm to 2.5 µm

By varying the six parameters y_0, λ_0, A, t_1, p *et* t_2 while comparing them with the actual solar spectrum; equation (1) then becomes :

$$ECL(\lambda) = 0{,}06977 + 7{,}0625\left[1 - e^{\frac{-(\lambda-0{,}26052)}{0{,}15994}}\right]^{2{,}28411} e^{\frac{-(\lambda-0{,}26052)}{0{,}22285}} \quad [kW.m^{-2}.\mu m^{-1}] \quad (2)$$

ISSN: 2356-5608

10.051103/IJSET.251220207
Vol.21 Iss.2 pp.70-87 **International Journal of Scientific Research & Engineering Technology (IJSET)**

The incident power and solar flux are respectively derived from the analytical expression of the solar irradiance as follows :

$$p_i = \int_{\lambda_{min}}^{\lambda_{max}} ECL(\lambda)\, d\lambda \quad [W.cm^{-2}] \tag{3}$$

$$\emptyset(\lambda) = \frac{ECL(\lambda)}{h\nu} \quad [cm^{-2}.s^{-1}.\mu m^{-1}] \tag{4}$$

B. Optical parameters of the material

These are essential parameters for optoelectronic devices such as photovoltaic solar cells, as they govern the propagation of light within the component. Among these parameters, we can mention :

1) *Evolution of the energy bandgap in l'$In_xGa_{1-x}N$:* The energy bandgap of l'$In_xGa_{1-x}N$ can be expressed according to Vegard's law, which relates the bandgap values of indium nitride (InN) and gallium nitride (GaN). Consequently, the $In_xGa_{1-x}N$ ternary alloy, formed from these two binary semiconductors (GaN and InN), possesses a direct bandgap that ranges from 0.7 eV to 3.42 eV. Vegard's law is an empirical rule stating that the lattice properties of an alloy (such as the energy bandgap, lattice parameters, etc.) can be determined through a linear interpolation of the property values of its constituent components. This law is defined by the following equation [10] :

$$E_g(In_xGa_{1-x}N) = xE_g(InN) + (1-x)E_g(GaN) \tag{5}$$

However, for the InGaN alloy bandgap, the measured values are not in full agreement with those obtained through linear interpolation. Consequently, a bowing parameter b is introduced into the expression to match the experimental data. Thus, Vegard's law, incorporating the bowing parameter b, is defined as follows [11] :

$$E_g(In_xGa_{1-x}N) = xE_g(InN) + (1-x)E_g(GaN) - bx(1-x) \tag{6}$$

Where $E_g(In_xGa_{1-x}N)$ represents the bandgap energy of the InGaN alloy [ev], $E_g(InN)$ et $E_g(GaN)$ are the energy bandgaps of InN et GaN, x is the indium concentration in $In_xGa_{1-x}N$ et b the bowing parameter. It is therefore important to specify its evolution as a function of temperature, which is given by the following Varshni expression [12] :

$$E_g = (1-x) * \left(3{,}51 - \frac{0{,}909.10^{-3} * T^2}{T+830}\right) + x * \left(0{,}72 - \frac{0{,}245.10^{-3} * T^2}{T+624}\right) - 1{,}43 * x * (1-x) \tag{7}$$

2) *Absorption coefficient:* Thus, for solar cell fabrication, materials with high absorption coefficients are preferred. The expression for the absorption coefficient α(λ) of InGaN can be found in various literature sources. In the present study, we have adopted the relationship where the absorption coefficient is given by [13] :

$$\alpha(\lambda, x) = 10^5 \sqrt{C(x)\left(E_{ph} - E_g(x)\right) + D(x)(E_{ph} - E_g(x))^2} \quad [cm^{-1}] \tag{8}$$

Where $E_{ph} = \frac{1{,}24}{\lambda}$ represents the photon energy, and λ is the wavelength,

$C(x) = 3{,}525 - 18{,}29 * x + 40{,}22 * x^2 - 37{,}52 * x^3 + 12{,}77 * x^4$; $D(x) = -0{,}6651 + 3{,}616 * x - 2{,}46 * x^2$

3) *Refractive index*: It is a highly influential factor for photovoltaic applications, as it allows for an increase in the absorption efficiency of a solar cell to achieve higher performance. The refractive index of the $In_xGa_{1-x}N$ alloy is given by [14] :

$$n(\lambda, x) = \sqrt{A\left(\frac{E_{ph}}{E_g}\right)^{-2}\left[2 - \sqrt{1 + \frac{E_{ph}}{E_g}} - \sqrt{1 - \frac{E_{ph}}{E_g}}\right] + B} \tag{9}$$

Where depend on the material composition and are given by :

$$A(In_xGa_{1-x}N) = 13{,}55x + 9{,}31(1-x)$$

$$B(In_xGa_{1-x}N) = 2{,}05x + 3{,}03(1-x)$$

C. Electronic parameters of the material

ISSN: 2356-5608

10.051103/IJSET.251220207
Vol.21 Iss.2 pp.70-87 **International Journal of Scientific Research & Engineering Technology (IJSET)**

One of the most important objectives in describing a semiconductor with respect to its electrical and optical properties is to determine both carrier concentrations and energy distributions. This requires knowledge of the density of available states. Consequently, the electronic properties of a material stem from its energy bandgap, *Eg*, and its carrier density.

The intrinsic carrier concentration is related to the indium composition by the following relationship [15] :

$$n_i = \sqrt{N_c N_v}.e^{\frac{-E_g}{2K_B T}} \quad [cm^{-3}] \tag{10}$$

Where N_c and N_v are the densities of states in the conduction and valence bands, respectively. Their expressions are given by the following relationships :

$$N_c = \big(0{,}9x + 2{,}3(1-x)\big).10^{18} \quad [cm^{-3}]$$
$$N_v = \big(5{,}3x + 1{,}8(1-x)\big).10^{19} \quad [cm^{-3}]$$

$K_B = 1{,}38\ 10^{-23}\ J.K^{-1}$ represents the Boltzmann constant and T [K] the temperature. The effective mass of the carriers [kg] is expressed as follows [16] :

$$\begin{cases} \mathrm{m_n(In_xGa_{1-x}N)} = 0{,}12\mathrm{x} + 0{,}2(1-\mathrm{x}) \\ \mathrm{m_h(In_xGa_{1-x}N)} = 0{,}17\mathrm{x} + 1{,}0(1-\mathrm{x}) \end{cases} \tag{11}$$

Mobility is a critical material characteristic, as it reflects the ability of carriers to move within the material. Charge carrier mobility depends on numerous parameters such as temperature, doping levels, and carrier-carrier or carrier-impurity scattering. These mobility dependencies can be calculated using the analytical and empirical model proposed by Caughey and Thomas [17]. Thus, the electron mobility, μ_n, and the hole mobility, μ_p, are given by the following relationships :

$$\mu_{\mathrm{n}} = \mu_{\mathrm{min,n}}\left(\frac{\mathrm{T}}{300}\right)^{\alpha_{\mathrm{n}}} + \frac{\mu_{\mathrm{max,n}}\left(\frac{\mathrm{T}}{300}\right)^{\beta_{\mathrm{n}}} - \mu_{\mathrm{min,n}}\left(\frac{\mathrm{T}}{300}\right)^{\alpha_{\mathrm{n}}}}{1+\left(\frac{\mathrm{N_n}}{\mathrm{N_n^{crit}}\left(\frac{\mathrm{T}}{300}\right)^{\gamma_{\mathrm{n}}}}\right)^{\delta_{\mathrm{n}}}} \tag{12}$$

$$\mu_{\mathrm{p}} = \mu_{\mathrm{min,p}}\left(\frac{\mathrm{T}}{300}\right)^{\alpha_{\mathrm{p}}} + \frac{\mu_{\mathrm{max,p}}\left(\frac{\mathrm{T}}{300}\right)^{\beta_{\mathrm{p}}} - \mu_{\mathrm{min,p}}\left(\frac{\mathrm{T}}{300}\right)^{\alpha_{\mathrm{p}}}}{1+\left(\frac{\mathrm{N_p}}{\mathrm{N_p^{crit}}\left(\frac{\mathrm{T}}{300}\right)^{\gamma_{\mathrm{p}}}}\right)^{\delta_{\mathrm{p}}}} \tag{13}$$

Where T is the temperature [K], $N_{n,p}$ the carrier concentration $[cm^{-3}]$, $\alpha, \beta\ et\ \gamma$ are set to 1 when experimental data are not available [18]. $\delta, \mu_{\mathrm{min,n,p}}, \mu_{\mathrm{max,n,p}}\ et\ \mathrm{N_{n,p}^{crit}}$ are empirical parameters specific to each semiconductor. Their values are reported in table I.

TABLE I : PARAMETERS USED IN THE CALCULATION OF CARRIER MOBILITY AS A FUNCTION OF DOPING CONCENTRATION AND TEMPERATURE [19], [16]

Carriers	**Parameters**	values
Electrons	$\mu_{\mathrm{min,n}}[\mathrm{cm^2.V^{-1}.s^{-1}}]$	55
	$\mu_{\mathrm{max,n}}[\mathrm{cm^2.V^{-1}.s^{-1}}]$	1000
	$\gamma_{\mathrm{n}}[\mathrm{s.d}]$	1
	$\mathrm{N_n^{crit}}[\mathrm{cm^{-3}}]$	2.10^{17}
Holes	$\mu_{\mathrm{min,p}}[\mathrm{cm^2.V^{-1}.s^{-1}}]$	3
	$\mu_{\mathrm{max,p}}[\mathrm{cm^2.V^{-1}.s^{-1}}]$	170
	$\gamma_{\mathrm{p}}[\mathrm{s.d}]$	2
	$\mathrm{N_p^{crit}}[\mathrm{cm^{-3}}]$	3.10^{17}

D. Generation rate and recombination rate

ISSN: 2356-5608

10.051103/IJSET.251220207
Vol.21 Iss.2 pp.70-87 **International Journal of Scientific Research & Engineering Technology (IJSET)**

The operation of a solar cell is based on the generation and separation of electron-hole pairs through light absorption. However, recombination of these electron-hole pairs always occurs, limiting the cell's performance. Consequently, in a semiconductor material, a given recombination mechanism is characterized by a recombination rate, which represents the number of recombinations per unit of time and per unit of volume.

The overall expression for the electron-hole pair generation rate $G_{n,p}(z,\lambda)$ at a distance from the illuminated surface of the cell, under monochromatic illumination in steady-state conditions, is given by the following relationship [9] :

$$G_{n,p}(z,\lambda) = \alpha(\lambda)\emptyset(\lambda)(1-R(\lambda))e^{-\alpha(\lambda)z} \quad (14)$$

Where $\emptyset(\lambda)$ represents the solar flux, $\alpha(\lambda)$ et $R(\lambda)$ represent the absorption and reflection coefficients, respectively.

To model the losses within the structure, we take into account Shockley-Read-Hall (SRH) recombination. Thus, the recombination rate can be defined as a function of the minority carrier density as follows [12], [9] :

$R_n(z) = \frac{n(z)}{\tau_n}$ is the electron recombination rate in the P-region (15)

$\mathrm{R_p(z)} = \frac{\mathrm{n(z)}}{\tau_\mathrm{p}}$ is the hole recombination rate in the N-region (16)

Where $\mathrm{n(z)}$ is the electron concentration in the P-region and $\mathrm{p(z)}$ is the hole concentration in the N-region, which are obtained by solving the continuity and transport equations under steady-state conditions ; τ_n and τ_p represent the electron and hole lifetimes, respectively.

The dependence of the SRH model lifetime on doping and defect density is given by the following relationship [20], [21] :

$$\tau_{\mathrm{n,p}} = \frac{\tau_{0(\mathrm{n,p})}}{1+{\mathrm{N_{total}}}/{\mathrm{N_{(n,p)}^{SRH}}}} \quad (17)$$

With

- $\tau_{0(\mathrm{n,p})} = 10^{-7}$ s : reference lifetimes for electrons and holes, independent of the defect density defined in the material.
- $\mathrm{N_{total}}$: total concentration of defect and doping impurities [$\mathrm{cm^{-3}}$]
- $\mathrm{N_{(n,p)}^{SRH}} = 5.10^{16}\mathrm{cm^{-3}}$: constant defining the recombinant defect concentrations for electrons and holes.

E. Photocurrent density $J_{ph}(\lambda)$

The photocurrent density, or volume photocurrent density, is a vector that describes the electric current at a local scale, at every point within the cell.

Based on the continuity equations that describe the temporal variations of charge densities (electrons, holes), we write, for electrons in the P-type semiconductor [22] :

$$G_n - R_n + \frac{1}{q}.\frac{dJ_n}{dz} = \frac{dn}{dt} \quad (18)$$

In the case of an N-type semiconductor, the minority carriers are holes, and the continuity equation is written as follows :

$$\mathrm{G_p - R_p - \frac{1}{q}.\frac{dJ_p}{dz} = \frac{dp}{dt}} \quad (19)$$

Where n and p are the electron and hole concentrations, J_n and J_p are the electron and hole current densities, G_n and G_p are the electron and hole generation rates, R_n and R_p are the electron and hole recombination rates, which themselves have complex expressions, particularly related to the illumination level, and q is the elementary charge.

Since we are working under steady-state conditions, these equations become :

$$\mathrm{G_n - R_n + \frac{1}{q}.\frac{dJ_n}{dz} = 0} \quad (20)$$

$$\mathrm{G_p - R_p - \frac{1}{q}.\frac{dJ_p}{dz} = 0} \quad (21)$$

ISSN: 2356-5608

10.051103/IJSET.251220207
Vol.21 Iss.2 pp.70-87 **International Journal of Scientific Research & Engineering Technology (IJSET)**

The electron and hole current densities (J_n and J_p) are obtained from the transport equations. Thus, the movement of charge carriers occurs either under the influence of an electric field or due to a charge carrier concentration gradient.

Summing the two types of currents (drift and diffusion currents) allows us to obtain the total current density for electrons and holes as follows [23] :

$$J_n = n.q.\mu_n.E + q.D_n.\frac{dn}{dz} \quad (22)$$

$$\mathrm{J_p} = \mathrm{p.q.\mu_p.E} - \mathrm{q.D_p}.\frac{\mathrm{dp}}{\mathrm{dz}} \quad (23)$$

With E is the electric field, μ_n and μ_p the electron and hole mobilities, respectively, D_n and D_p represent the electron and hole diffusion coefficients, respectively, and are defined by the Einstein relation [24] :

$$D_n = \frac{K_B T}{q}\mu_n \quad (24)$$

$$\mathrm{D_p} = \frac{\mathrm{K_B T}}{\mathrm{q}}\mu_\mathrm{p} \quad (25)$$

1) *Current density in the P-type quasi-neutral region:* When the doping is uniform and neutral, the electric field becomes zero throughout these regions but is non-zero within the space charge region (SCR). The expression describing the phenomena in the emitter region, obtained by substituting the expressions for G_n, R_n and J_n, is given as follows :

$$\alpha.\emptyset(1-R).e^{-\alpha.z} - \frac{n}{\tau_n} + D_n\frac{d^2n}{dz^2} = 0 \quad (26)$$

After solving, the general solution of this equation is the sum of the homogeneous equation solution and the particular solution, and is given by the following relation :

$$\mathrm{n(z)} = \mathrm{A_1.\cosh\left(\frac{z}{L_n}\right) + B_1.\sinh\left(\frac{z}{L_n}\right) - \frac{\alpha.\emptyset(1-R).\tau_n}{\alpha^2.L_n^2-1}.e^{-\alpha.z}} \quad (27)$$

Where $\mathrm{L_n} = \sqrt{\mathrm{D_n\tau_n}}$ represents the electron diffusion length, $\mathrm{A_1}$ and $\mathrm{B_1}$ are constants to be determined from the boundary conditions.

- At the cell surface, recombination occurs with a recombination velocity S_n :

$$D_n\frac{dn(z)}{dz} = S_n\,.n(z) \qquad en\ z = 0 \quad (28)$$

- At the junction boundary, the excess carrier density is reduced to zero by the electric field within the depletion region, which is expressed as :

$$n(z) = 0 \quad en\ z = z_j \quad (29)$$

$\mathrm{A_1}$ and $\mathrm{B_1}$ are determined from these two boundary conditions, which will allow us to obtain the expression for the electron density n(z) in the following form :

$$n(z) = \left[\frac{\alpha.\emptyset(1-R).\tau_n}{\alpha^2.L_n^2-1}\right]\left[\frac{\left(\frac{S_nL_n}{D_n}+\alpha L_n\right)sinh\left(\frac{z_j-z}{L_n}\right)+e^{-\alpha z_j}\left(\left(\frac{S_nL_n}{D_n}\right)sinh\left(\frac{z}{L_n}\right)+cosh\left(\frac{z}{L_n}\right)\right)}{\left(\frac{S_nL_n}{D_n}\right)sinh\left(\frac{z_j}{L_n}\right)+cosh\left(\frac{z_j}{L_n}\right)} - e^{-\alpha z}\right] \quad (30)$$

The expression for the photocurrent density $\mathrm{J_n(\lambda)}$ is obtained from the minority carrier density n(z). It is defined by the following relation :

$$\mathrm{J_n(\lambda) = q.D_n.\left(\frac{dn(z)}{dz}\right)_{z_j}} \quad (31)$$

This implies that the photocurrent is expressed as follows :

$$\mathrm{J_n(\lambda) = \left[\frac{qF(1-R)\alpha L_n}{\alpha^2{L_n}^2-1}\right]\left[\frac{\left(\frac{S_nL_n}{D_n}+\alpha L_n\right)-e^{-\alpha z_j}\left(\left(\frac{S_nL_n}{D_n}\right)cosh\left(\frac{z_j}{L_n}\right)+sinh\left(\frac{z_j}{L_n}\right)\right)}{\left(\frac{S_nL_n}{D_n}\right)sinh\left(\frac{z_j}{L_n}\right)+cosh\left(\frac{z_j}{L_n}\right)} - \alpha L_n e^{-\alpha x_j}\right]} \quad (32)$$

This current density is the emitter's contribution to the total photocurrent at a given wavelength.

ISSN: 2356-5608

10.051103/IJSET.251220207
Vol.21 Iss.2 pp.70-87 **International Journal of Scientific Research & Engineering Technology (IJSET)**

2) *Current density in the N-type quasi-neutral region:* In the N-type semiconductor, the minority carriers are holes. Thus, by substituting the expressions for G_p, R_p and J_p, the continuity equation in this region is written as follows :

$$\frac{d^2p}{dz^2} - \frac{p}{L_p^2} = -\frac{1}{D_p}.\alpha.\emptyset(1-R).e^{-\alpha.z} \quad (33)$$

After solving, the general solution of this equation is the sum of the homogeneous solution and the particular solution, and is given by the following relation :

$$p(z) = A_2.\cosh\left(\frac{z}{L_p}\right) + B_2.\sinh\left(\frac{z}{L_p}\right) - \frac{\alpha.\emptyset(1-R).\tau_p}{\alpha^2.L_p^2-1}.e^{-\alpha.z} \quad (34)$$

Where $L_p = \sqrt{D_p\tau_p}$ represents the hole diffusion length, A_2 and B_2 are constants that can be determined from the following boundary conditions :

- Just as in the emitter region, at the edge of the depletion region, the excess minority carrier density is zero :
$$p(z) = 0 \quad \text{en } z = z_j + w \quad (35)$$
- At the back surface of the cell, recombination occurs with a velocity S_p, the condition for which is as follows : S_p
$$-D_p\frac{dp(z)}{dz} = S_p p(z) \quad \text{en} \quad z = H \quad (36)$$

By applying these boundary conditions, the hole density p(z) in the base is written as follows :

$$p(z) = \left[\frac{\alpha.\emptyset(1-R).\tau_p}{\alpha^2.L_p^2-1}\right]e^{-\alpha(z_j+w)}\left\{\cosh\left(\frac{z-z_j-w}{L_p}\right) - e^{-\alpha(z-z_j-w)} - \right.$$
$$\left. SpLpDpcoshH'Lp-e-\alpha H'+sinhH'Lp+\alpha Lpe-\alpha H'SpLpDpsinhH'Lp+coshH'Lpsinhz-zj-wLp\right\} \quad (37)$$

The hole photocurrent $J_p(\lambda)$ at the junction is written as follows :

$$J_p(\lambda) = -q.D_p.\left(\frac{dp(z)}{dz}\right)_{z_j+w} \quad (38)$$

By utilizing this relation ; $J_p(\lambda)$ is written in the following form :

$$J_p(\lambda) = \left[\frac{qF(1-R)\alpha L_p}{\alpha^2 {L_p}^2-1}\right]e^{-\alpha(z_j+w)}\left\{\alpha L_p - \frac{\left(\frac{S_pL_p}{D_p}\right)\left[\cosh\left(\frac{H'}{L_p}\right)-e^{-\alpha H'}\right]+\sinh\left(\frac{H'}{L_p}\right)+\alpha L_p e^{-\alpha H'}}{\left(\frac{S_pL_p}{D_p}\right)\sinh\left(\frac{H'}{L_p}\right)+\cosh\left(\frac{H'}{L_p}\right)}\right\} \quad (39)$$

Avec $H' = H - (z_j + w)$

$$w = \sqrt{\frac{2\varepsilon}{q}.\frac{N_a+N_b}{N_aN_b}.V} \quad (40)$$

$$V = V_T ln\left(\frac{N_aN_b}{n_i^2}\right) \quad (41)$$

$$V_T = \frac{K_BT}{q} \quad (42)$$

Where V_T represents the thermal voltage (J/C) or Volt, V the built-in potential at the junction in Volts, N_a and N_b represent the doping levels in the P and N layers, respectively [cm^{-3}].

3) *Current density in the space charge region:* In the space charge region, the continuity equation for electrons is written as follows :

$$G_n - R_n + \frac{1}{q}\frac{dJ_{ZCE}}{dz} = \frac{dn}{dt} \quad (43)$$

ISSN: 2356-5608

10.051103/IJSET.251220207
Vol.21 Iss.2 pp.70-87 **International Journal of Scientific Research & Engineering Technology (IJSET)**

With J_{ZCE} being the current generated in the space charge region.

In steady-state conditions and neglecting recombination phenomena in this region, the continuity equation becomes :

$$G_n + \frac{1}{q}\frac{dJ_{ZCE}}{dz} = 0 \quad \rightarrow \quad J_{ZCE} = -q\int_{z_j}^{z_j+w} G_n dz \tag{44}$$

By replacing G_n with its expression $\alpha.\emptyset(1-R).e^{-\alpha.z}$ and by integrating, we obtain J_{ZCE} in the following form :

$$J_{ZCE}(\lambda) = -q.\emptyset(1-R).e^{-\alpha.z_j}(1-e^{-\alpha w}) \tag{45}$$

Consequently, the total photocurrent density is given by :

$$J_{ph}(\lambda) = J_n(\lambda) + J_p(\lambda) + J_{ZCE}(\lambda) \tag{46}$$

The total photocurrent density Jph is obtained by integrating the current density $J_{ph}(\lambda)$ over the entire range of the solar spectrum ($AM_{1,5G}$).

F. Characteristic Parameters of the Solar Cell

The current-voltage (J-V) characteristic of the cell is given by the following equation [25], [12], [11] :

$$J = J_{ph} - J_{obsc} = J_{ph} - J_0\left(e^{\frac{qV}{K_BT}} - 1\right) \tag{47}$$

Where :

- J_{ph} = the photo-generated current [A]
- J_{obsc} the diode dark current [A]
- $J_0 = qn_i^2(\frac{D_p}{L_pN_d} + \frac{D_n}{L_nN_a})$ is the diode saturation current [A]
- D_n and D_p minority carrier diffusion coefficients in the P and N regions, respectively [cm^2s^{-1}]
- L_n and L_p the diffusion lengths in the P and N layers, respectively [cm]
- N_d and N_a the doping levels in the N and P materials [cm^{-3}]
- $q = 1{,}602.10^{-19}C$ the elementary charge of an electron
- V the voltage across the diode [V]
- $K_B = 1{,}38.10^{-23}\,J.K^{-1}$ the Boltzmann constant
- T the temperature in Kelvin

From the (J-V) characteristic, we can easily deduce the short-circuit current density J_{sc}, the open-circuit voltage V_{oc} and the maximum power P_m, given respectively by :

$$J_{sc} = J_{ph} \tag{48}$$

$$V_{oc} = \frac{K_BT}{q} ln\left(\frac{J_{cc}}{J_0} + 1\right) \tag{49}$$

$$P_m = V_m * J_m \tag{50}$$

Thus, the fill factor and the conversion efficiency are deduced from the following equations :

$$FF = \frac{P_m}{J_{cc}V_{oc}} = \frac{J_mV_m}{J_{cc}V_{oc}} \tag{51}$$

$$\eta = \frac{P_m}{P_{inc}} = \frac{J_m*V_m}{P_{inc}} = \frac{FF*I_{cc}*V_{oc}}{E*S} \tag{52}$$

With S being the cell area and E the illumination or irradiance in $W.m^{-2}$.

IV. Preliminary Results

The electrical characterization of a photovoltaic cell is essential for evaluating its performance. The current-voltage J(V) and power-voltage P(V) curves allow for the extraction of key parameters such as the open-circuit voltage (Voc), the short-circuit current density (Jsc) and the maximum power (Pmax). Thus, the simulation is performed using Matlab/Simulink software. We simulate the characteristics of a so-called 'reference' photovoltaic cell and an identical cell coupled with a resonant optical structure composed of thin dielectric layers. The objective is to compare their performances to determine the impact of this structure on the overall efficiency of the cell.

ISSN: 2356-5608

10.051103/IJSET.251220207
Vol.21 Iss.2 pp.70-87 International Journal of Scientific Research & Engineering Technology (IJSET)

The current-voltage J(V) and power-voltage P(V) characteristics of the reference cell are shown in Fig. 2 and Fig. 3 below, respectively.

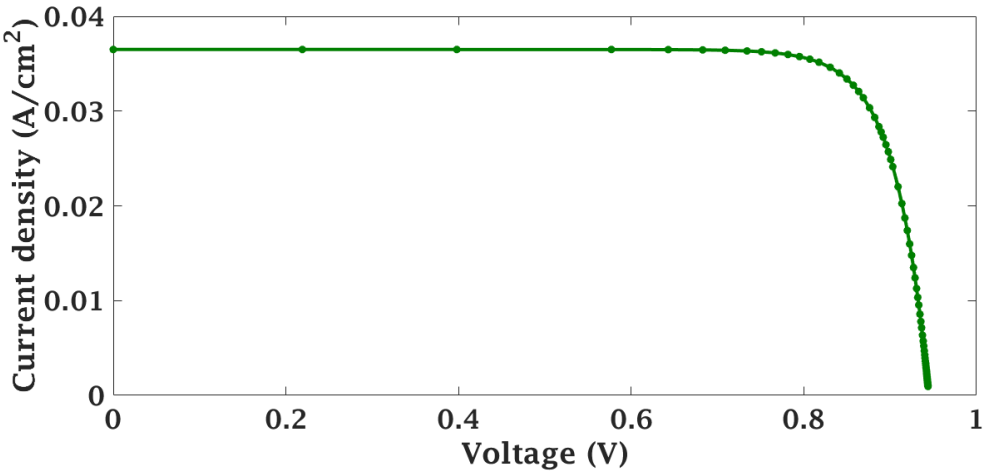

Fig. 2 Current-voltage characteristic of the reference cell

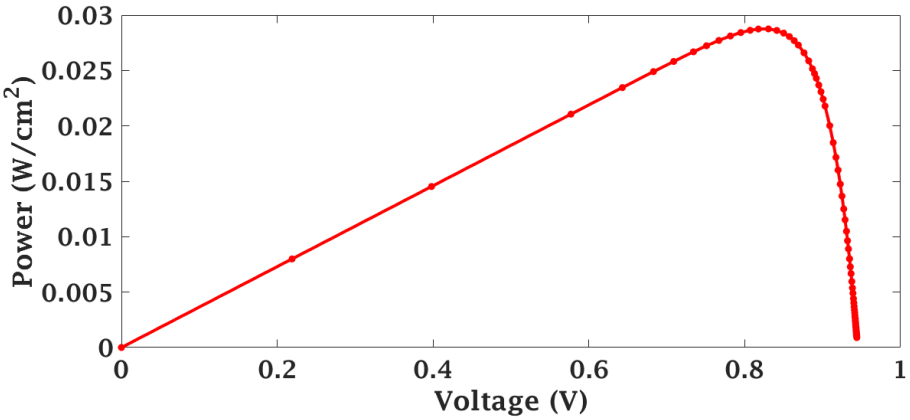

Fig. 3 Power-voltage characteristic of the reference cell

To highlight the impact of integrating the resonant structure into the conventional solar cell used as a reference, we simulated the J(V) and P(V) characteristics of the modified cell, presented in Fig. 4 and Fig. 5, respectively. These results are obtained from the optimal values of $Na = 2{,}86.10^{18}\,cm^{-3}$ and of $Nd = 5{,}66.10^{17}\,cm^{-3}$ and non-optimal emitter and base thicknesses, which are respectively 195 nm and 1020 nm.

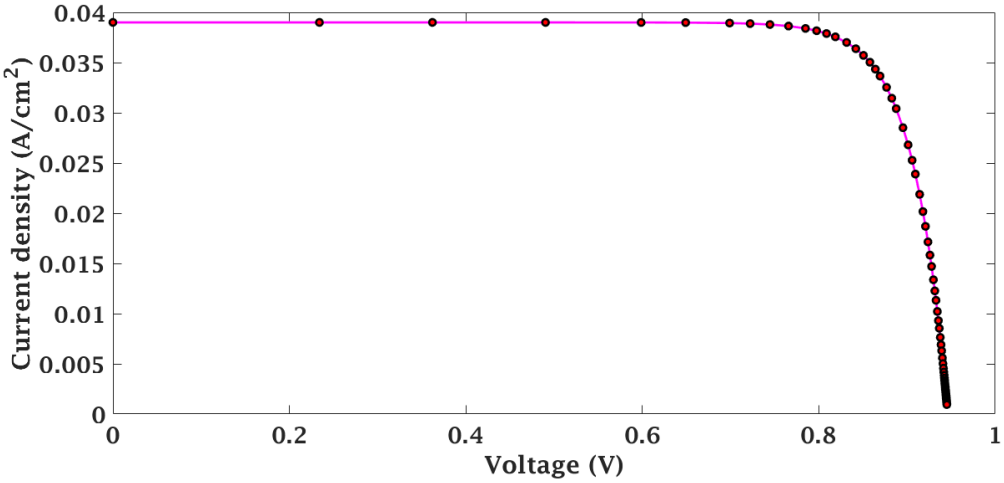

Fig. 4 Current-voltage characteristic of the coupled cell

ISSN: 2356-5608

10.051103/IJSET.251220207
Vol.21 Iss.2 pp.70-87 International Journal of Scientific Research & Engineering Technology (IJSET)

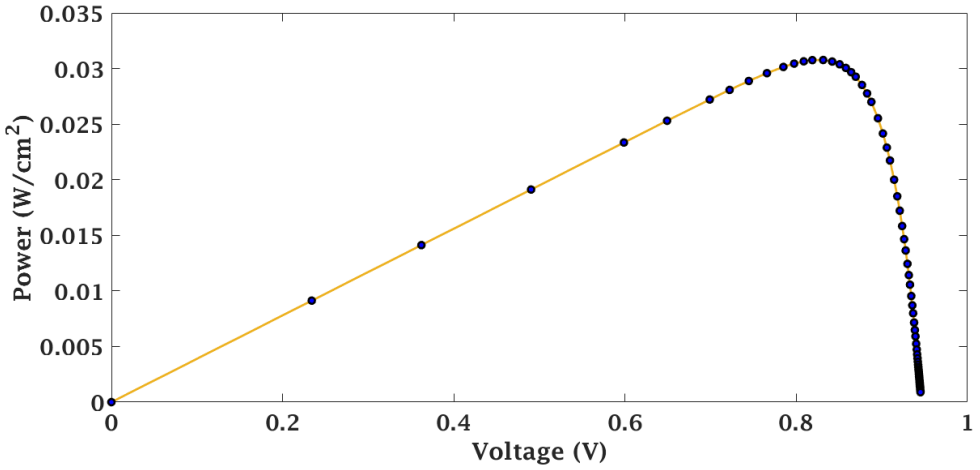

Fig. 5 Power-voltage characteristic of the coupled cell

The different output parameters of these two cells are summarized in Table II below.

TABLE II OUTPUT PARAMETERS OF THE REFERENCE CELL AND THE COUPLED CELL

	Jsc (mA/cm^2)	**Voc (V)**	**Pmax (mW/cm^2)**	**Ƞ (%)**
Reference cell	32,68	0,94	26,51	26,50
Coupled cell	39	0,946	30,7	30,7

The simulated J(V) and P(V) curves show a clear improvement in the maximum extracted power for the cell with the multi-dielectric structure. The short-circuit current increases significantly, reflecting better photon collection in the spectral region optimized by the resonant structure. This leads to an increase in efficiency from 26.50% to 30.70%.

To further improve this efficiency, we will proceed with the optimization of the emitter and base thicknesses of the coupled cell.

V. OPTIMIZATION OF THE CONVERSION EFFICIENCY

In order to further optimize the conversion efficiency of this coupled cell, we will improve it by studying the influence of the thicknesses of its various layers.

1) *Effect of the emitter thickness*: The effect of varying the emitter thickness (p-layer) on the cell's performance is studied over a thickness range between 0,01 and 1 μm. Emitter doping Na and that of the base Nd are fixed at $2{,}86.10^{18}\,cm^{-3}$ and at $5{,}66.10^{17}\,cm^{-3}$ respectively, as well as the base thickness at 1020 nm. The Fig. 6, Fig. 7 and Fig. 8 illustrate respectively the cell parameters ($V_{co}, J_{cc}\ et\ \eta$) as a function of the thickness (z_j).

ISSN: 2356-5608

10.051103/IJSET.251220207
Vol.21 Iss.2 pp.70-87 International Journal of Scientific Research & Engineering Technology (IJSET)

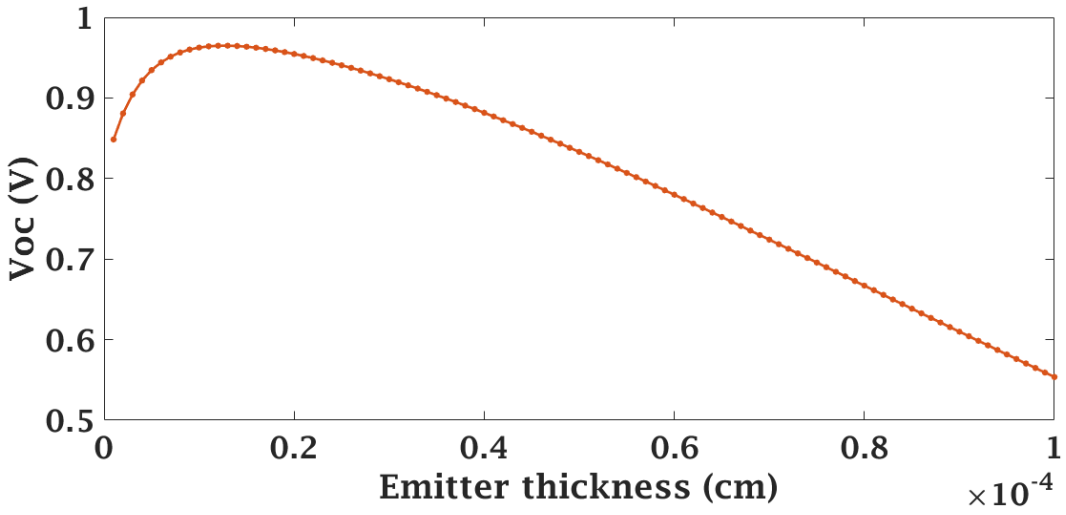

Fig. 6 Open-circuit voltage (Voc) as a function of emitter thickness

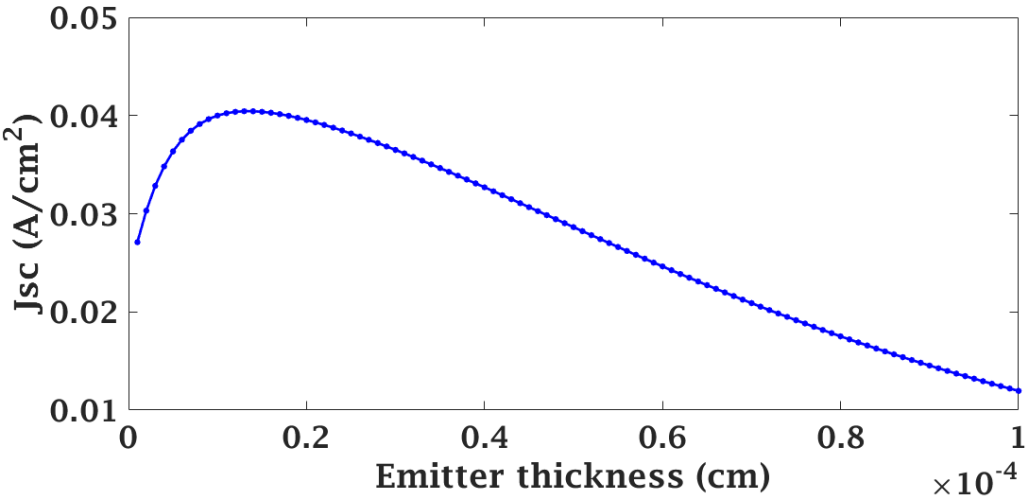

Fig. 7 Short-circuit current density (Jsc) as a function of emitter thickness

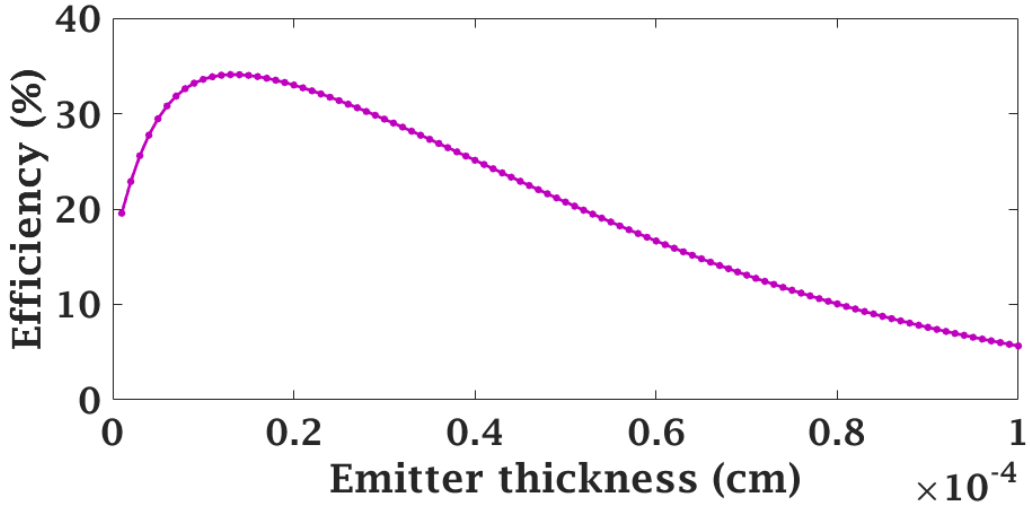

Fig. 8 Conversion efficiency (ɳ) as a function of emitter thickness

ISSN: 2356-5608

10.051103/IJSET.251220207
Vol.21 Iss.2 pp.70-87 International Journal of Scientific Research & Engineering Technology (IJSET)

The obtained results (Fig. 7 and Fig. 8) show that the short-circuit current density (Jsc) and the conversion efficiency ((ɳ)) first increase and then decrease with the increase of the emitter thickness. This produces the same behavior for the open-circuit voltage (Voc).

On the one hand, the short-circuit current density (Jsc) increases as the emitter thickness decreases. This is because the distance between the Space Charge Region (SCR) and the surface where recombination occurs is reduced, thereby improving the carrier collection efficiency in this zone. This leads to an increase in (Jsc) up to a maximum value of 41 $mA.cm^{-2}$. This means that as the emitter becomes thinner and thinner, a large amount of photons across the entire spectrum (from wavelengths near the bandgap ~ 893 nm to shorter wavelengths) can be absorbed by the base.

On the other hand, the collection efficiency of the Space Charge Region (SCR) is weakened when it is very close to the surface, where surface recombination effects occur. This reduction in collection efficiency leads to a decrease in the short-circuit current density (Jsc), the conversion efficiency (ɳ), and also the open-circuit voltage (Voc).

It is observed that the efficiency (ɳ) and the short-circuit current density (Jsc) reach peak values at the same thickness, $z_j = 130\text{nm}$, corresponding to a maximum conversion efficiency of approximately 34.08%. The maximum value reached by the open-circuit voltage is 0.96 V.

2) *Effect of the base thickness*: In this section, we varied the base thickness from 0.3 to 4 μm to observe its influence on the cell's performance. The other parameters, such as the emitter doping Na, the base doping Nd, and the emitter thickness z_j, were set to the optimized values obtained from the previous studies in this work. This influence is illustrated in Fig. 9, 10 and 11 below.

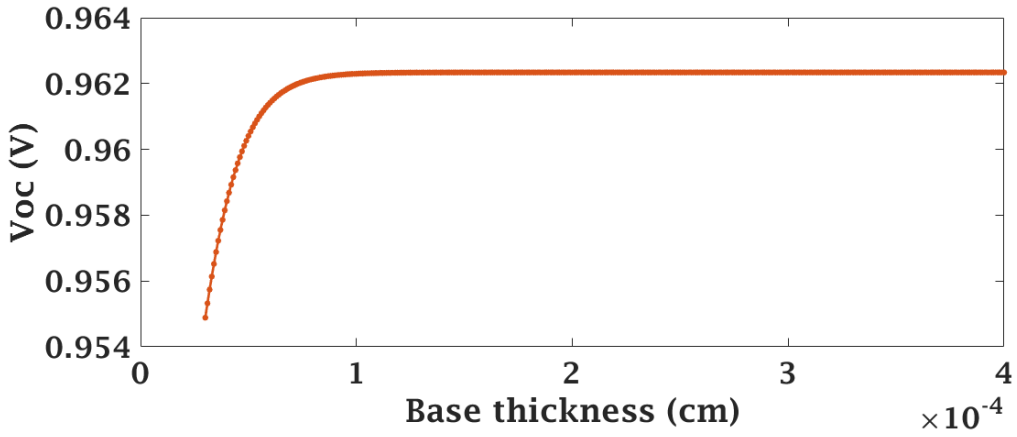

Fig. 9 Open-circuit voltage (Voc) as a function of base thickness

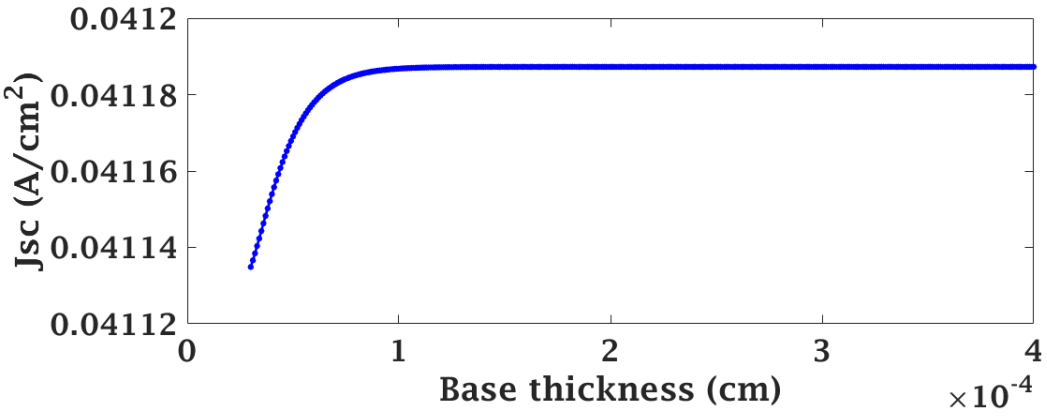

Fig. 10 Short-circuit current density (Jsc) as a function of base thickness

ISSN: 2356-5608

10.051103/IJSET.251220207
Vol.21 Iss.2 pp.70-87 International Journal of Scientific Research & Engineering Technology (IJSET)

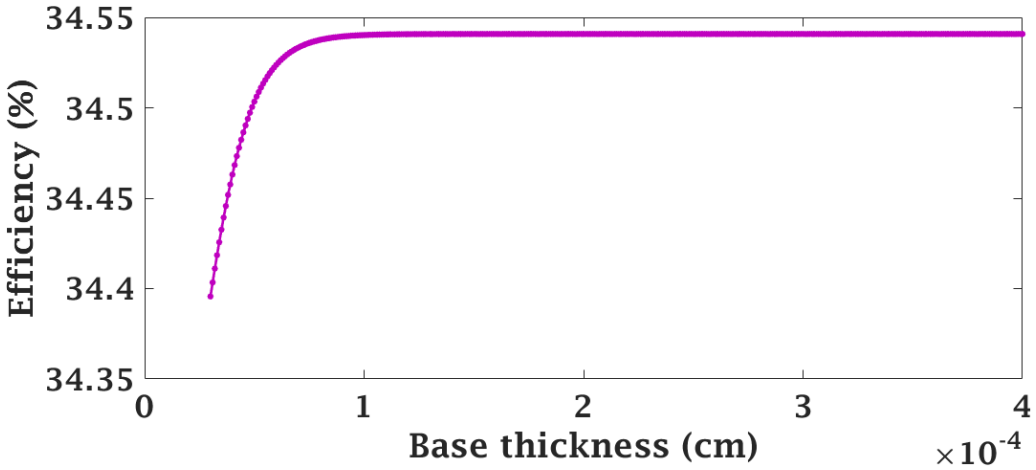

Fig. 11 Conversion efficiency (ɳ) as a function of base thickness

Figs. 9, 10, and 11 illustrate respectively the variations of the open-circuit voltage (V_{oc}), the short-circuit current density (J_{sc}), and the efficiency (ɳ) as a function of the base thickness. Based on these results, an improvement in the different cell parameters is observed as the base thickness increases. For the open-circuit voltage (V_{oc}) and the short-circuit current density (J_{sc}), we obtain respectively $0{,}9623\,V$ and $41{,}2\,mA.cm^{-2}$. With a base thickness of 820 nm, a maximum conversion efficiency ($\eta = 34.54\,\%$) is obtained and remains constant beyond this value. This thickness is sufficient to exploit a wide range of the solar spectrum. However, the cell's electrical parameters are less affected by the base thickness compared to those of the emitter.

3) *Optimal performance of the solar cell*: The optimal values obtained after the parametric study are as follows :

- The doping concentration of the P-layer (acceptor) is $Na = 2{,}86.10^{18}\ cm^{-3}$
- The doping concentration of the N-layer (donor) is $Nd = 5{,}66.10^{17}\ cm^{-3}$

The thicknesses of the acceptor and donor layers are 820 nm and 130 nm, respectively.

Based on these results, we were able to determine the current-voltage J(V) and power-voltage P(V) characteristics of the optimized solar cell under illumination $AM_{1.5}$ $(0{,}1W/cm^2)$ and at a temperature of $(T = 300\ K)$. Thus, the J(V) and P(V) characteristics resulting from this simulation are shown in Fig. 12 and Fig. 13, respectively.

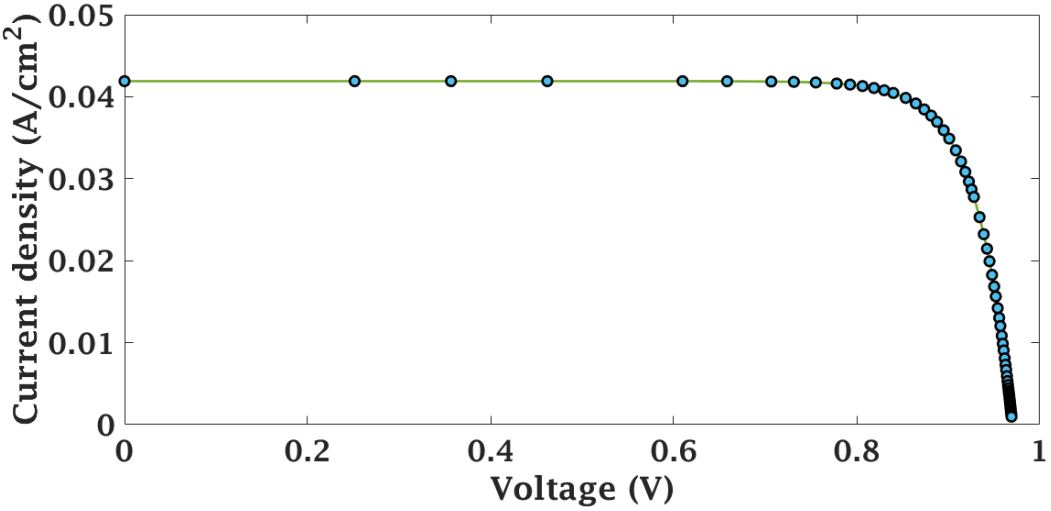

Fig. 12 Current-voltage (J-V) characteristic of the optimized cell

ISSN: 2356-5608

10.051103/IJSET.251220207
Vol.21 Iss.2 pp.70-87 International Journal of Scientific Research & Engineering Technology (IJSET)

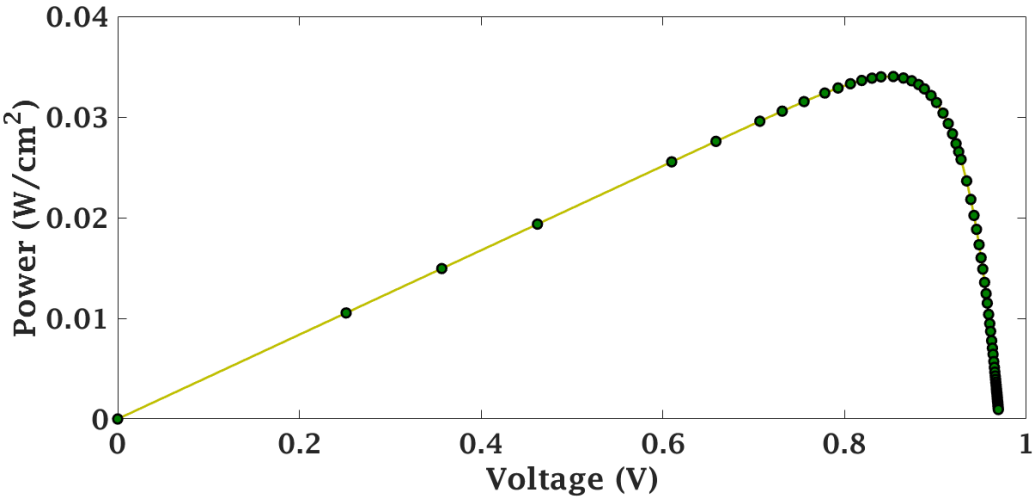

Fig. 13 Power-voltage (P-V) characteristic of the optimized cell

From these two characteristics, we determined the parameters of the optimized solar cell, which are presented in table III.

TABLE III OUTPUT PARAMETERS OF THE OPTIMIZED COUPLED SOLAR CELL

Parameters	Values
$V_{co}(V)$	0,962
$J_{cc}(mA.cm^{-2})$	41,20
$P_{max}(mW.cm^{-2})$	34,54
ɳ (%)	34,54

4) *Comparison between the reference cell, the coupled cell, and the optimized coupled cell:* To evaluate the performance of the model used, a comparative study was conducted between the control cell (reference), the coupled cell, and the optimized InGaN-based coupled cell. Figs. 14 and 15 illustrate the current-voltage J(V) and power-voltage P(V) characteristics of these three configurations, respectively.

ISSN: 2356-5608

10.051103/IJSET.251220207
Vol.21 Iss.2 pp.70-87 International Journal of Scientific Research & Engineering Technology (IJSET)

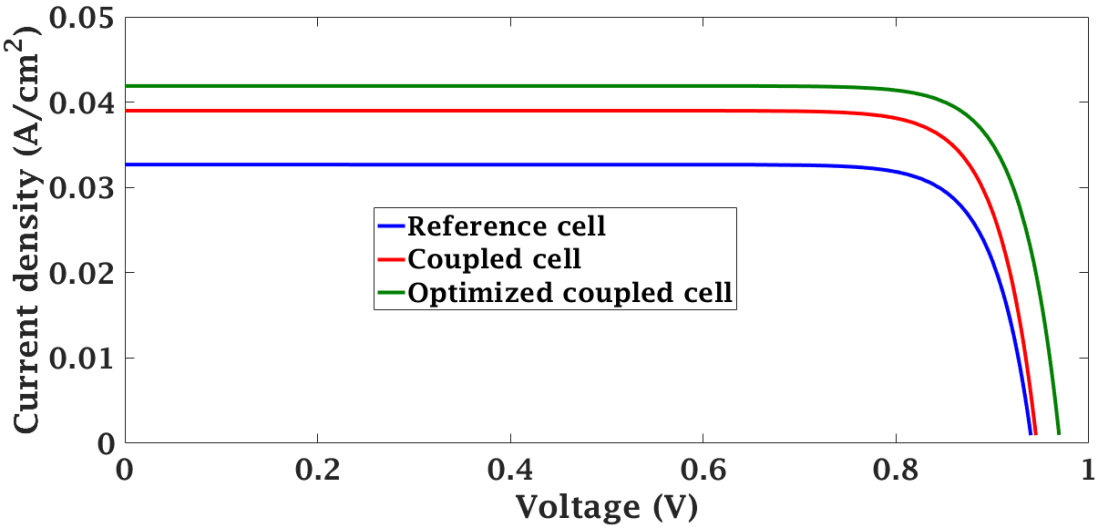

Fig. 14 Current-voltage characteristics of the three cells

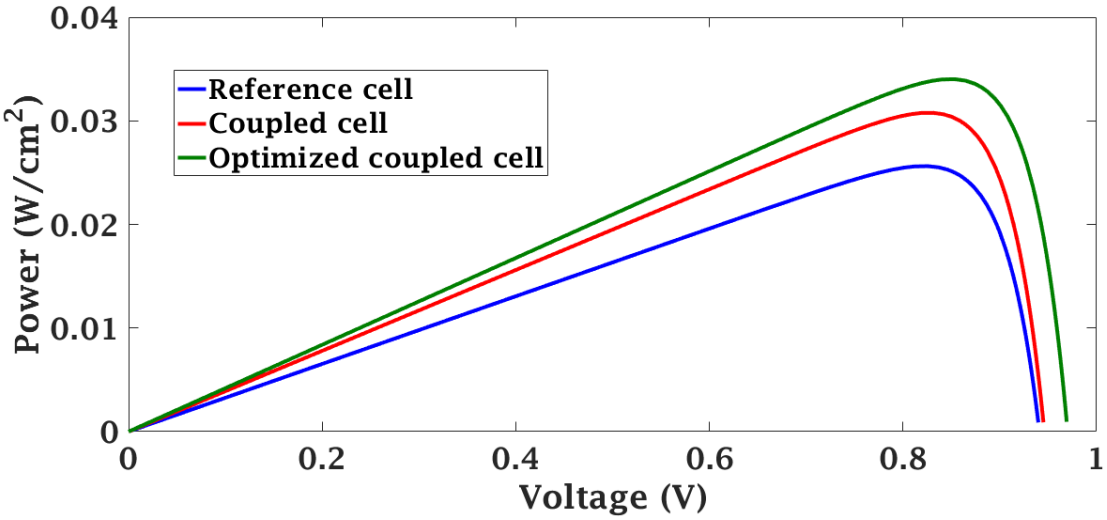

Fig. 15 Power-voltage characteristics of the three cells

The analysis of these three curves highlights an improvement in the current-voltage J(V) and power-voltage P(V) characteristics, ranging from the control cell to the optimized coupled cell. The main photovoltaic parameters of the three structures are summarized in the comparative table IV below.

TABLE IV OUTPUT PARAMETERS OF THE THREE CELLS

	Jsc (mA/cm^2)	**Voc (V)**	**Pmax (mW/cm^2)**	**Ƞ (%)**
Reference Cell	32,68	0,94	26,51	26,50
Coupled Cell	39	0,946	30,7	30,7
Optimized Coupled Cell	41,20	0,962	34,54	34,54

ISSN: 2356-5608

According to the data in table IV, it is clear that the photovoltaic performance of the optimized coupled solar cell surpasses those of both the standard coupled cell and the control cell. The improvement is particularly significant in terms of short-circuit current (Jsc) and conversion efficiency (η). The integration of the resonant structure, followed by the optimization of the emitter and base thicknesses, allows for an increase in the short-circuit current from 32,68 mA·cm^{-2} to 41,20 mA·cm^{-2}, while the efficiency increases from 26.50% to 34.54%. These gains are attributed to the amplification of the optical field before its interaction with the front surface of the cell, as well as to the optimized thicknesses of the emitter and the base. These results confirm the significance of photonic approaches for the optimization of next-generation solar cells.

VI. CONCLUSION

In this paper, we have undertaken an in-depth modeling of a single-junction solar cell based on Indium Gallium Nitride (InGaN), integrated into a multi-dielectric resonant structure, under multi-spectral illumination and in a steady-state regime. Through simulations conducted using Matlab/Simulink, we identified optimal doping and thickness configurations for the emitter and base layers. This optimization led to a conversion efficiency of 34.54%, representing a significant improvement over the initial performance.

These results underscore the promising potential of wide-bandgap materials such as InGaN for the fabrication of high-efficiency solar cells, particularly when integrated into advanced optical architectures like resonant structures. The study also highlights the critical role of the emitter thickness in the overall cell performance, providing a clear pathway for future optimization strategies.

REFERENCES

[1] R. Adib, *, "Renewables 2015 Global Status Report," 2015.*, vol. 4, no. 3. 2015.
[2] S. Endo, S. Kimura, T. Takatsuji, K. Nanasawa, T. Imanaka, and K. Shizuma, "Measurement of soil contamination by radionuclides due to the Fukushima Dai-ichi Nuclear Power Plant accident and associated estimated cumulative external dose estimation," *J. Environ. Radioact.*, vol. 111, pp. 18–27, 2012.
[3] Y. Lahiouel, S. Latreche, and M. Khemliche, "Adaptive neuro fuzzy inference system based method for faults detection in the photovoltaic system," *Indones. J. Electr. Eng. Comput. Sci.*, vol. 32, no. 2, pp. 773–786, 2023.
[4] S. Latreche, M. Mostefai, M. Khemliche, and A. E. Badoud, "Implementation of a MPPT algorithm and supervision of a shading on photovoltaic panel," *2015 6th Int. Renew. Energy Congr. IREC 2015*, vol. 8, no. 6, pp. 3541–3544, 2015.
[5] M. A. Hessad, Z. Bouchama, S. Benaggoune, and K. Behih, "Cascade sliding mode maximum power point tracking controller for photovoltaic systems," *Electr. Eng. Electromechanics*, vol. 2023, no. 1, pp. 51–56, 2023.
[6] C. B. Lim, "GaN / AlGaN heterostructures for infrared optoelectronics : polar vs nonpolar orientations Caroline Botum Lim HAL Id : tel-01693891," 2019.
[7] A. Adaine, S. Ould, S. Hamady, and N. Fressengeas, "Effects of structural defects and polarization charges in InGaN-based double-junction solar cell," *Superlattices Microstruct. Elsevier*, vol. 107, pp. 267–277, 2017.
[8] P. François, K. Tagne, K. Kenfack, and A. Dimitri, "Journal of Renewable Energies," vol. 24, pp. 25–39, 2021.
[9] A. Benmir and M. S. Aida, "Analytical modeling and simulation of CIGS solar cells," *Energy Procedia*, vol. 36, pp. 618–627, 2013.
[10] G. F. Brown, J. W. Ager, W. Walukiewicz, and J. Wu, "Finite element simulations of compositionally graded InGaN solar cells," *Sol. Energy Mater. Sol. Cells*, vol. 94, no. 3, pp. 478–483, 2010.
[11] C. A. Hernández-Gutiérrez, A. Morales-Acevedo, D. Cardona, G. Contreras-Puente, and M. López-López, "Analysis of the performance of InxGa1−xN based solar cells," *SN Appl. Sci.*, vol. 1, no. 6, 2019.
[12] L. Mousli, B. Dennai, and B. Azeddine, "THEORETICAL SIMULATION OF THE EFFECT OF TEMPERATURE OF MULTI-JUNCTION SOLAR CELLS (PIN / InGaN)," vol. 17, no. 1, pp. 11–21, 2021.
[13] A. Mesrane, A. Mahrane, F. Rahmoune, and A. Oulebsir, "Optimal band gaps for InGaN single and double junction solar cells," *Proc. Int. Conf. Adv. Syst. Electr. Technol. IC_ASET 2017*, no. 2, pp. 335–339, 2017.
[14] "Semiconductor Optoelectronic Devices | ScienceDirect." [Online]. Available: https://www.sciencedirect.com/book/9780080469782/semiconductor-optoelectronic-devices. [Accessed: 29-Aug-2024].
[15] "(PDF) Etude et Optimisation des Cellules Solaires Tandem à Haut Rendement Ga0.2 Al0.8 As-Ga0.68 Al0.32 As-Ga As, avec Trois Sorties." [Online]. Available: https://www.researchgate.net/publication/279770912_Etude_et_Optimisation_des_Cellules_Solaires_Tandem_a_Haut_Rendement_Ga02_Al08_As-Ga068_Al032_As-Ga_As_avec_Trois_Sorties. [Accessed: 29-Aug-2024].
[16] A. Mesrane, F. Rahmoune, A. Mahrane, and A. Oulebsir, "Design and Simulation of InGaN p-n Junction Solar Cell," *Int. J. Photoenergy*, vol. 2015, p. 9, 2015.
[17] D. M. Caughey and R. E. Thomas, "Carrier mobilities in silicon empirically related to doping and field," *Proc. IEEE*,

ISSN: 2356-5608

vol. 55, no. 12, pp. 2192–2193, 1967.
[18] A. Adaine *et al.*, "InGaN Metal-IN Solar Cell : optimized efficiency and fabrication tolerance To cite this version : HAL Id : hal-01523416," *China Fr. Second. Adv.*, 2018.
[19] X. Zhang *et al.*, "Simulation of In0.65Ga0.35 N single-junction solar cell," *J. Phys. D. Appl. Phys.*, vol. 40, no. 23, pp. 7335–7338, 2007.
[20] Silvaco, "Silvaco User's Manual DEVICE SIMULATION SOFTWARE," no. October, 2004.
[21] M. Razeghi and M. Henini, "Optoelectronic Devices: III Nitrides," *Optoelectron. Devices III Nitrides*, pp. 1–575, Jan. 2005.
[22] "Joachim Piprek - Google Scholar." [Online]. Available: https://scholar.google.com/citations?user=z5x6A1IAAAAJ&hl=en. [Accessed: 29-Aug-2024].
[23] "J.S. Yuan - Google Scholar." [Online]. Available: https://scholar.google.com/citations?user=b-C_s6gAAAAJ&hl=en. [Accessed: 29-Aug-2024].
[24] M. Joseph, *Fundamentals of Semiconductor Physics, Hamburg, Anchor Academic Publishing*. 2015.
[25] Y. Marouf, L. Dehimi, F. Bouzid, F. Pezzimenti, and F. G. D. Corte, "Theoretical design and performance of InxGa1-xN single junction solar cell," *Optik (Stuttg).*, vol. 163, pp. 22–32, 2018.

ISSN: 2356-5608